A Pen-Pressure-Sensitive Capacitive Touch System Using Electrically Coupled Resonance Pen

Changbyung Park, Sungsoo Park, Ki-Duk Kim, *Student Member, IEEE*, Sanghui Park, *Student Member, IEEE*, Juwan Park, Byunghoon Kang, Yunhee Huh, and Gyu-Hyeong Cho, *Senior Member, IEEE*

***Abstract*—A touch system sensing pen-pressure of the proposed electrically coupled resonance (ECR) pen is implemented, which can replace costly digitizer system containing electro magnetic resonance (EMR) and capacitive touch system. The proposed system detects the location of the ECR pen and finger using proposed position sensor, and senses pen-pressure of ECR pen using proposed pen-pressure sensor. For the position sensor, to detect even small variation of the mutual capacitance on touch screen panel (TSP) of the pen, a simultaneous driving scheme is proposed with modified Hadamard matrix, resulting in highly increased dynamic range and SNR. In the proposed pen-pressure sensor, the resonant frequency of the ECR pen is measured by a frequency to voltage converter based sensor. The measured SNR for the pen position is 49 dB with 1 mm φ metal pillar, and 6.5-bit resolution is achieved for pen-pressure sensor in 6σ criteria.**

***Index Terms*—Capacitive, pen, pen-pressure, resonance, touch screen.**

I. Introduction

INTUITIVE and interactive interface, capacitive touch screens are widely adopted in mobile devices. There are several types of touch screens such as resistive, capacitive, acoustic, optical, and so on [1]. Among these types of the touch screens, capacitive touch screens have overwhelmed the others due to its durability, sleek design, optical clearness, and superior touch performance. There are two types in the capacitive touch screens [2]. The first is self-capacitive touch screen which has a touch information in the capacitance between a single sensing electrode and ground. When the conductive object like finger is touched, the self-capacitance increases due to additional capacitance between the sensing electrode and the object. Read-out circuits detect this capacitance variation and finds touched point. The second is mutual-capacitive touch screen which has touch information in the capacitance matrix between transmitting (TX) electrodes and receiving (RX) electrodes. When the touch screen panel (TSP) is touched, the corresponding capacitance between TX and RX electrodes decreases, and the variation is sensed by the sensing circuit. Since the mutual-capacitive touch screen supports multi-touch UX (user experience) that can detect several touched points on TSP at the same time, whereas the self-capacitive touch screen suffers from ghost touch problem using TSP [2].

Touch screen controllers suffer from external noise sources such as display noise, hum, charger noise, etc., which degrade signal to noise ratio (SNR) of the system and cause coordinate jitter. To overcome these noises, [3] adopted integrating structure, which integrates multiple charges from a TSP. The noises are averaged and filtered by expensing sensing time. In the mutual capacitive TSP, the capacitance is composed of two parts, a static component and a dynamic component. The static component is a kind of offset (base) capacitance which does not change whether the sensing node of the TSP is touched or not. The dynamic component is varying part of the mutual capacitance depending on the touch. Since [3] integrates the charge containing the static component, an external integrating capacitor is required to process the large amount of charge from the TSP.

Integrating structure can efficiently reduce the influence of the external noises by means of averaging the noise over time. Some noise sources, however, are common over RX electrodes of TSP. If the touch controller rejects these common noises, the SNR can be further enhanced. [4]–[6] adopted differential sensing scheme which integrates the RX incoming charge-difference between adjacent RX electrodes. Because the controllers only sense the charge-difference, the common mode noises and the static component of mutual capacitance are nullified and canceled out.

There is another scheme to improve the SNR. Multi-TX schemes [7], [8] simultaneously drive multitudinous TX electrodes. By doing so, RX incoming charge into the controller increases i.e. the signal strength that contains touch information is stronger than a single-TX scheme, thereby increasing TX driving power. The driving patterns are based on orthogonal matrices such as Hadamard, pseudorandom noise (PN) sequence, and so on to calculate a mutual capacitance matrix from coded charges into RX. However the RX incoming charge for the particular part of the matrix of this scheme is too large to process with on-chip capacitors and the number of charge integration to filter out the noise is limited, when the entire dozens of TX electrodes are driven simultaneously. The high order matrix calculation for the mutual capacitance matrix gives also large computing burden.

Using these kinds of schemes, the SNR of the controllers have been sufficiently improved against the external noises, and the up-to-date commercial touch controllers offer excellent UX.

Manuscript received April 23, 2015; revised June 12, 2015; accepted June 28, 2015. This paper was approved by Guest Editor Yusuke Oike.

C. Park is with Samsung Electronics, Suwon, Korea. He is also with KAIST, Daejeon, Korea.

S. Park, J. Park, and B. Kang are with Samsung Electronics, Suwon, Korea.

K.-D. Kim, S. Park, Y. Huh, and G.-H. Cho are with KAIST, Daejeon, Korea

Color versions of one or more of the figures in this paper are available online at http://ieeexplore.ieee.org.

Digital Object Identifier 10.1109/JSSC.2015.2453943

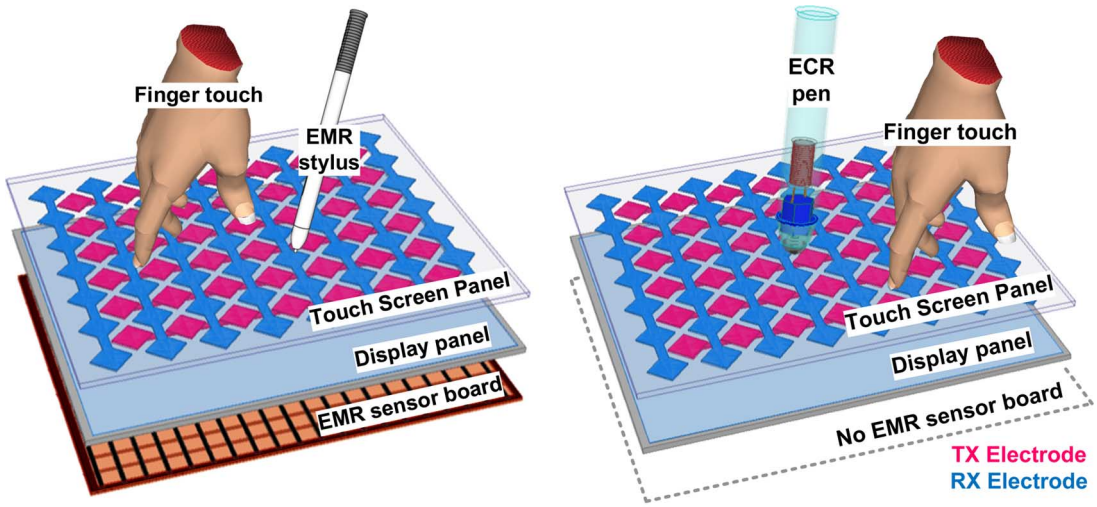

(a) (b)

Fig. 1. Sensing panel configuration of (a) EMR system with a capacitive touch screen, and (b) proposed ECR pen touch system.

Beyond the ordinary capacitive touch system, consumers need more advanced one. To satisfy these needs, some devices adopt an extra electro magnetic resonance (EMR) system [9] to support pen-function, and have been successfully commercialized for high-end devices [10]. It offers realistic and accurate pen drawing experience with battreryless, light, and pen-pressure-sensitive stylus, because the EMR system excites the stylus via magnetic coupling and senses stylus' returning signal that contains coordinate and pen-pressure information with a passive stylus. Different from capacitive touch screen based system, the EMR system needs an extra sensor board exploiting magnetic coupling between the EMR sensor board and the stylus. The sensor board is equipped at beneath the display panel of the mobile device as shown in Fig. 1(a). The sensor board that made with multi-layer flexible printed circuit board adds system complexity, thickness, and power consumption of its dedicated controller.

As another way of the pen-function, some devices adopt an active pen [11]. The feature of the active pen covers similar function of the EMR system such as pen-pressure sensing, button on a pen, short range hover, and so on. The active pen system does not require the extra sensor board for the stylus, but the pen is a stand-alone system which has function of Bluetooth, accelerometer, transmitter, rechargeable batteries, dedicated IC, and so on. Because of these active components, it is quite hard to make the active pen compact like the stylus of EMR system that can be put into a mobile phone, and the complex pen system adds overall system cost.

Considering these issues of the stylus system, we considered the following requirements of the pen solution.

1) The pen should be passive for the compact implementation.
2) No additional sensing board except conventional capacitive touch screen.

In this paper, cost effective and compact capacitive touch system that is not only compatible with finger touch but also covers the pen-pressure-sensitive passive pen only using conventional capacitive TSP without additional sensor board and its dedicated controller is proposed.

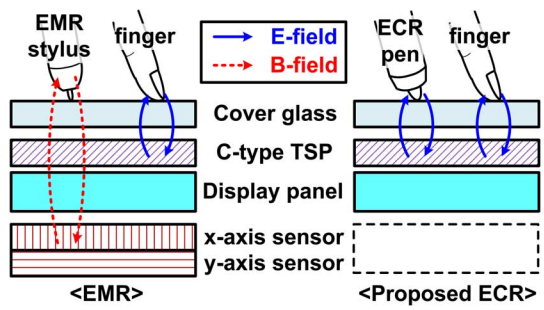

Fig. 2. Cross-sectional view comparison between the EMR system and proposed system.

II. Overall System Configuration

Fig. 1(b) shows sensing panel configuration of the proposed touch system. The proposed system does not require the EMR sensor board any more. The pen and fingers are sensed by a single capacitive TSP. Fig. 2 shows cross-sectional side view comparison between the EMR and the proposed ECR system. The proposed ECR pen is coupled with TSP via electric field, while the EMR stylus is coupled with EMR sensor board via magnetic field. Without EMR sensor board, the thickness of the sensors of the proposed system can be reduced.

The proposed system is separated into three parts, position sensor (PS), ECR pen, and pen-pressure sensor (PPS). To find touched points of ECR pen and fingers, position sensor constructs the mutual capacitance matrix using the proposed grouped multi-TX driving scheme. The ECR pen is composed of a conductive tip for the electric coupling and parallel LC resonant tank that is compose of pressure to capacitance transducer (P2CT) C_p and inductor L. In C_p, there is dielectric elastomer between conductive plates that are electrically connected as a capacitor. The elastomer is deformed with respect to applied pressure across C_p. The deformation changes physical dimension of the dielectric and C_p varies depending on applied pen-pressure, that results in the resonant frequency f_r variation of LC tank. f_r reflects the applied pen-pressure on the ECR pen.

Pen-pressure sensor senses this resonant frequency variation based on frequency to voltage converter.

III. Proposed Position Sensor

A. Multi-TX Scheme

To improve SNR of the touch system, RX incoming signal strength should be increased by means of increasing TX driving power, that are increasing TX driving voltage and simultaneous TX driving. In the proposed system, these two methods are adopted at the same time. Hadamard matrix is adopted for the driving patterns of the proposed system.

The example of the multi-TX scheme with the pattern of four simultaneous driving is shown in Fig. 3. The elements 1 s and -1 s of Hadamard matrix corresponds to rising and falling edge of the TX driving pulses, respectively. Each output voltage of the sensing circuit V_p is determined from the TX driving pattern corresponding to each pattern (single column of Hadamard matrix). After four times of sensing, one by four matrix $\boldsymbol{V}_p$ is constructed, and $\boldsymbol{C}_M$ can be found by multiplying $\boldsymbol{H}_4^{-1}$.

The proposed multi-TX driving pattern based on 8th order Hadamard matrix $\boldsymbol{H}_8$ is shown in Fig. 4. Whereas the conventional multi-TX schemes drives entire dozen of TX electrodes at the same time, eight TX electrodes are simultaneously driven to limit amount of RX incoming charge, reduce computing burden, and take an advantage in a local scanning. However there is problem adopting Hadamard matrix as it is. The first column of $\boldsymbol{H}_8$ is filled with only 1 s, and the other columns are well balanced with 1 s and -1 s (same number of 1 s and -1 s for each column). Even though the number of simultaneously driven TX electrodes is reduced to eight, RX incoming charge corresponding to the unbalanced first column is too large to be integrated in an on-chip integrator, resulting in saturation. Modification in the driving pattern is needed. Hence in the modified $\boldsymbol{H}_8$, the first column is omitted and the remaining well balanced columns are only used in an actual driving pattern; the RX incoming charge through static components (offset) of C_Ms are autonomously canceled out by the balanced characteristic of the modified $\boldsymbol{H}_8$. Because only the dynamic components of C_Ms are sensed, an additional offset charge canceling scheme [12] is not required to enhance dynamic range of the sensor.

With the driving pattern based on the modified $\boldsymbol{H}_8$, it is not possible to calculate the exact values of C_Ms due to missing equation from the omitted driving pattern. Although there are eight unknown mutual capacitances ($C_{M0} \sim C_{M7}$) in seven equations, the touch image can be constructed using the relationships among C_Ms from the simultaneous equations. Because the number of TX electrodes on TSP is larger than eight, scanning process is needed to find entire relationships C_Ms on the TSP. To calculate the relationship between the adjacent simultaneous driving groups, there should be an overlapped TX electrode in the adjacent groups for the continuous and complete touch image as shown in Fig. 5.

Since the multi-TX scheme senses TSP several times in order to construct complete matrix to be calculated, the touch information is spread over time (sensing time). If the more TX electrodes are simultaneously driven, the longer sensing time is needed. During the sensing time, fast moving object

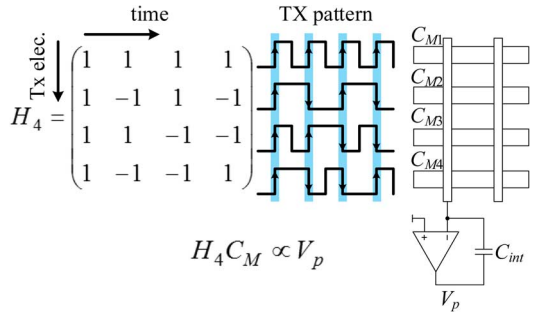

Fig. 3. Concept of multi-TX scheme.

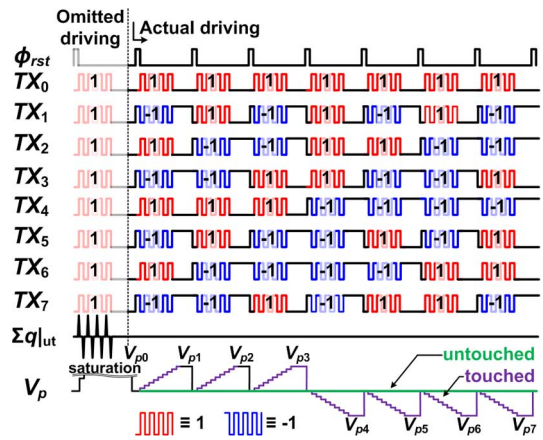

Fig. 4. Proposed multi TX driving pattern based on the modified Hadamard matrix.

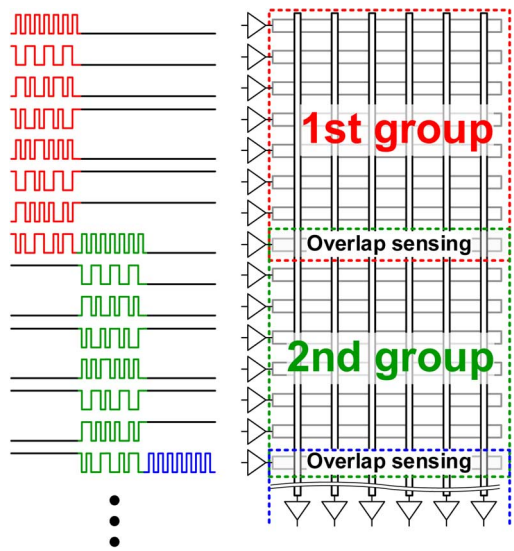

Fig. 5. Proposed scanning method.

on the TSP can cause error in the calculated touch coordinate. This problem is also relived in the proposed scheme due to the limited number of simultaneously driven electrodes.

B. Charge Demodulating Integrator

Fig. 6 shows charge demodulating integrator (CDI) of the position sensor. CDI integrates alternating RX incoming charge unidirectionally. CDI has two sensing modes. The one is absolute sensing mode (ASM) that integrates absolute amount of

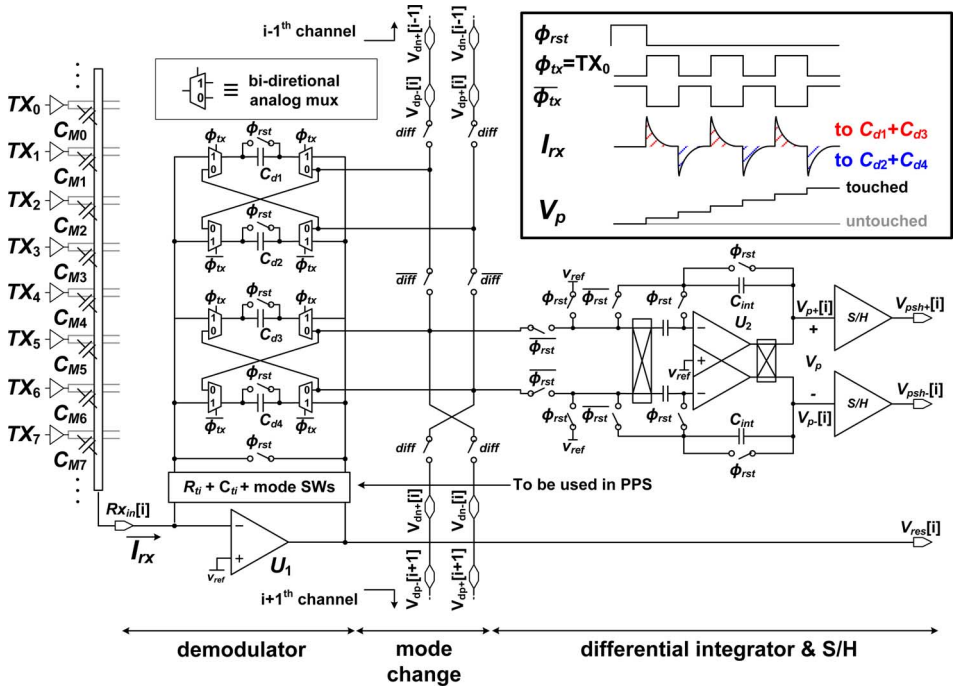

Fig. 6. Proposed charge demodulating integrator.

transferred charge from a single RX electrode to C_{int}, and the other is differential sensing mode (DSM) that integrates the charge difference between adjacent channels to nullify common mode noise [6]. Two modes are convertible depending on control bit $diff$. For example, CDI normally operates in ASM, and it changes its operating mode to DSM, depending on a noise level. For both modes, in demodulator, the RX incoming charges are stored in C_{d1} and C_{d3}, while the stored charges in C_{d2} and C_{d4} are transferred to integrator at $\varphi_{TX} = 1$, vice versa at $\varphi_{TX} = 0$, where capacitances of $C_{d1\sim4}$ are same.

In ASM, the charges in $C_{d1} + C_{d3}$ and $C_{d2} + C_{d4}$ are transferred to integrator, respectively. In DSM, the difference between the charge in C_{d4} (C_{d3}) of the current channel and that of C_{d2} (C_{d1}) of the next channel is integrated at $\varphi_{TX} = 1$ $(\varphi_{TX} = 0)$ by cross coupling of C_{d4} (C_{d3}) and C_{d2} (C_{d1}) at charge transferring to integrator, thereby the differential sensing is concurrently done without input multiplexing. There is no difference in Hadamard matrix processing between ASM and DSM. It is just the process multiplying Hadamard matrix to $\boldsymbol{V}_p$ matrix.

The charge transferring polarity of each phase is opposite to demodulate charge. Since the positive charge and the negative charge with inverting operation are summed and integrated to C_{int}, low frequency noise can be filtered [6] in both sensing modes. Normalized noise transfer function of the proposed CDI which integrates charges from both of TX driving edges can be calculated in z-domain as follows:

$$\frac{V_p(z)}{N(z)} = \frac{\sum_{i=1}^{2N_{int}} (-1)^i z^{-i}}{2N_{int}}, \tag{1}$$

where N_{int} is the number of TX driving pulses, and $(-1)^i$ term is from integrating both polarities of RX incoming charges. (1)

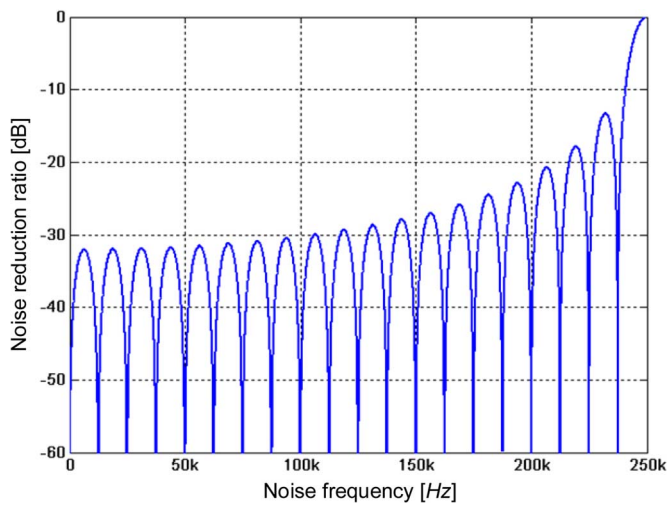

Fig. 7. Normalized noise transfer function plot of (1).

is plotted in Fig. 7, where TX driving frequency and N_{int} are 250 kHz and 20, respectively. As explained, the low frequency noise below TX driving frequency is effectively reduced.

If the CDI just integrates the charges from single edges of TX driving pulses, the normalized noise transfer function is changed as follows:

$$\left.\frac{V_p(z)}{N(z)}\right|_{\text{single edge}} = \frac{\sum_{i=1}^{N_{int}} z^{-2i}}{N_{int}} \tag{2}$$

(2) is plotted in Fig. 8, where TX driving frequency and N_{int} are 250 kHz and 20, respectively. In this case, the low frequency noise is not suppressed by the integrating procedure especially

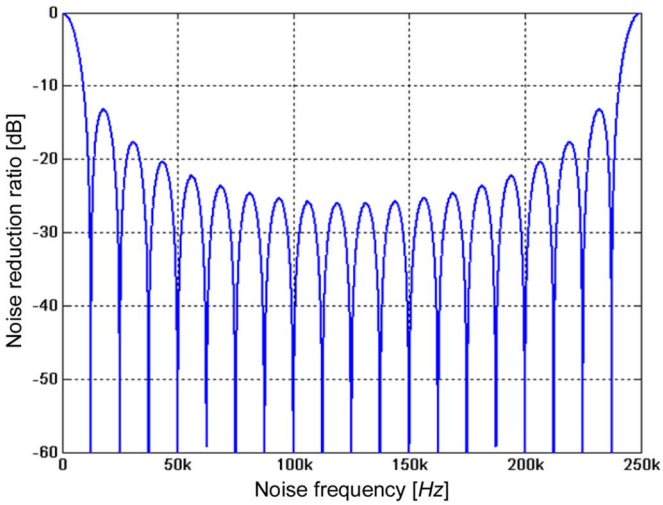

Fig. 8. Normalized noise transfer function plot of (2).

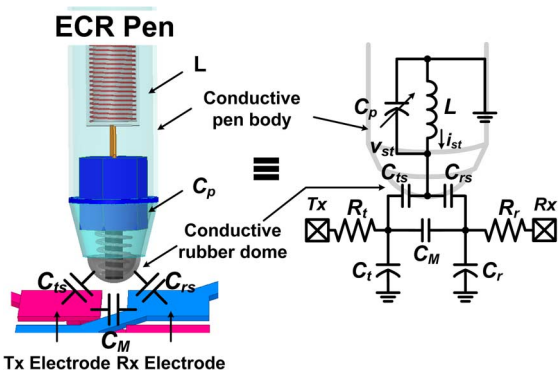

Fig. 9. ECR pen and circuit model.

near DC. In the low frequency band, there are hum and electronic ballast noise. Without further filtering this noise, SNR of the touch sensor can be severely degraded.

IV. Proposed Pen-Pressure Sensor

A. Operation of ECR Pen

Rough sketch of the ECR pen and its circuit model with TSP are shown in Fig. 9. Comparing with EMR pen, the most different thing is coupling method. EMR pen is coupled to its dedicated sensor board through magnetic coupling, while ECR pen is coupled to conventional capacitive TSP through electric field. Under this condition, there are some structural differences between them for the resonance in an LC tank. Inductor of the EMR pen is used for LC resonance as well as for the magnetic coupling. So the inductor is located at the tip of the pen. Since the ECR pen operates through electric coupling, an inductor is only used for the resonance; an inductor can be located any part in the pen. For the resonance, one terminal of LC tank in the ECR pen should be grounded and the other terminal should be connected to the conductive pen-tip that is coupled to capacitive TSP. In the ECR pen, pen-body is conductive and it is used as ground of the LC tank similarly with active styluses.

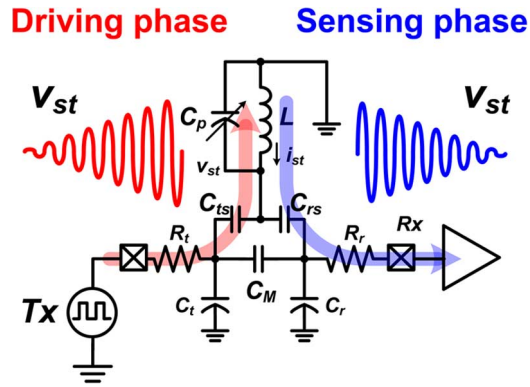

Fig. 10. Driving phase and sensing phase of the ECR pen.

The resonant frequency LC resonant tank of the ECR pen f_r is as follows:

$$f_r = \frac{1}{2\pi\sqrt{L(C_p + C_{ts}||C_{rs})}} \approx \frac{1}{2\pi\sqrt{LC_p}}, \qquad (3)$$

where C_{ts} and C_{rs} are coupling capacitance between the ECR pen and the electrodes of TSP. Because of small value of C_{ts} and C_{rs} compared to C_p, they are approximated in (3). Pen-pressure-sensor senses f_r to calculate the variation of C_p that corresponds applied pen-pressure on the ECR pen. Because the ECR pen is passive, the operation of the pen is separated into two phases, driving phase and sensing phase as shown in Fig. 10.

B. Operation of Pen-Pressure Sensor

Fig. 11 shows the detailed structure of pen-pressure sensor and its timing chart. After the position sensor finds touch coordinates of objects, pen-pressure sensing is performed separately. Depending on the touch coordinate, the nearest TX electrode to the coordinate is driven, and the output of the transimpedance amplifier U_1 that is shared amplifier in CDI is connected to pen-pressure sensor by an analog multiplexer. In driving phase, a driven TX electrode excites the resonant tank in the ECR pen with the predefined resonant frequency exploiting capacitive coupling, and resonant energy is charged in the resonant tank. In sensing phase, coming just after the end of driving a TX electrode, the resonant tank still resonates with the frequency of f_r and the resonant voltage vst at the conductive tip of the ECR pen is amplified to output of the transimpedance amplifier V_r. Offset compensated inverter based comparator converts V_r to digital signal $\boldsymbol{\varphi}_r$. The reference frequency of f_r is set to 500 kHz and pen-pressure sensor detects how much f_r is deviated from 500 kHz whose period is 2 μs. Phase frequency detector (PFD) detects phase difference between $\boldsymbol{\varphi}_r$ and 2 μs delayed $\boldsymbol{\varphi}_r$ ($\boldsymbol{\varphi}_{rd}$) through reference delay cell (RDC). For example, if the period of $\boldsymbol{\varphi}_r$ is longer than 2 μs, PFD generates up pulses whose pulse width is same as difference between the period of $\boldsymbol{\varphi}_r$ and 2 μs. To average and filter phase noise of $\boldsymbol{\varphi}_r$, differential integrator (DI) integrates the current pulses from differential charge pump (DCP) and Vpp is generated after the given number of integration. As shown in Fig. 11(b), Pen-pressure sensor performs

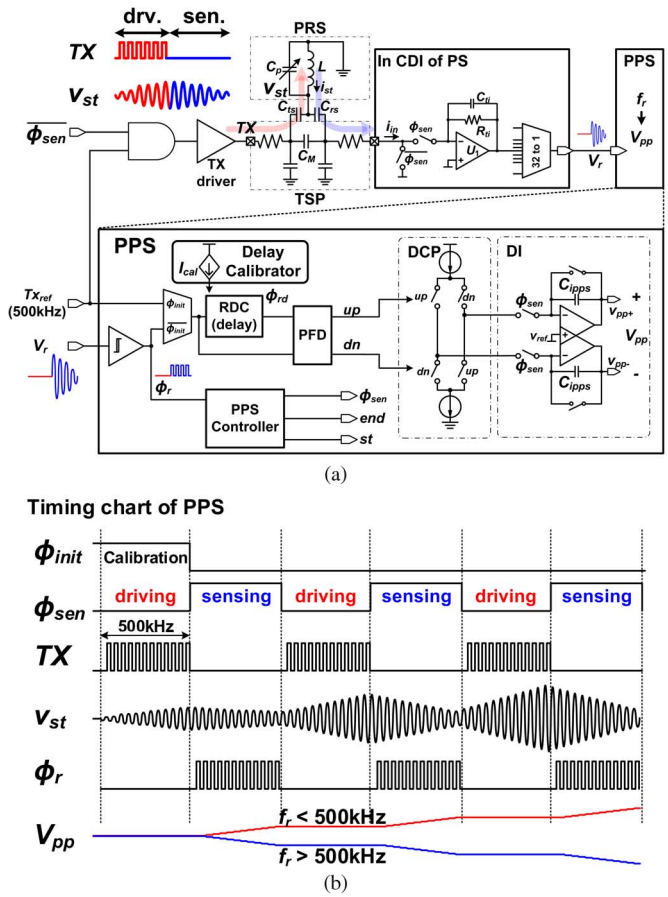

Fig. 11. (a) Proposed pen-pressure sensor and (b) its timing chart.

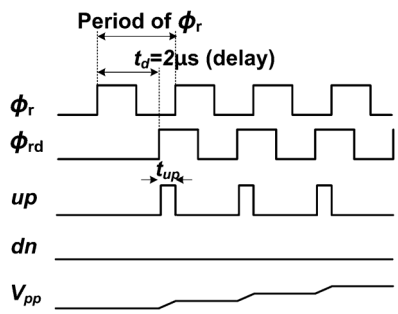

Fig. 12. Timing chart of the pen-pressure sensor for analysis.

this driving and sensing pair several times since it is hard to obtain enough noise performance and dynamic range at once due to short resonant sustaining time in the ECR pen.

Because the ECR pen can only resonate with designated frequency and finger cannot generate resonant signal, the system can discriminate the ECR pen on a TSP by means of counting the number of resonant pulses of φ_r. If the ECR pen is not detected i.e. fingers are touched after initial driving, pen-pressure sensor does not proceed the operation.

The detailed timing chart of pen-pressure sensor is shown in Fig. 12. The resonant period of the ECR pen T_r is as follows:

$$T_r = \frac{1}{f_r} = 2\pi\sqrt{LC_p}. \tag{4}$$

The pulse width of t_{up} that is phase difference between φ_r and φ_{rd} is as follows:

$$t_{up} = T_r - t_d, \tag{5}$$

where t_d is propagation delay of the reference delay.

V_{pp} can be calculated as follows:

$$V_{pp} = \frac{t_{up} I_{cp}}{C_{ipps}} N, \tag{6}$$

where N, I_{cp}, and C_{ipps} are the number of *up* pulses to be integrated, output current of charge pump, and capacitance of integrator, respectively. Substituting (5) to (6),

$$V_{pp} = \left\{ 2\pi\sqrt{L(C_{p0} + \Delta C_p)} - t_d \right\} \frac{I_{cp}}{C_{ipps}} N, \tag{7}$$

where C_{p0} and ΔC_p are the reference capacitance that makes f_r the reference resonant frequency 500 kHz, and variation of C_p from C_{p0}, respectively. Assuming

$$\Delta C_p << C_{p0}, \quad t_d = 2\pi\sqrt{LC_{p0}}, \tag{8}$$

V_{pp} can be derived with approximation as follows:

$$V_{pp} \cong \frac{\pi \Delta C_p \sqrt{LC_{p0}}}{C_{p0}} \cdot \frac{I_{cp}}{C_{int}} N \tag{9}$$

V_{pp} is proportional to small variation of ΔC_p.

C. Reference Delay Calibrator

Detailed structure of delay calibrator with its timing chart are shown in Fig. 13. The propagation delay of RDC should be calibrated to guarantee the accuracy of pen-pressure sensor, because RDC adopts current starved inverter chain (CSIC) that might be sensitive to PVT variations. Initializing phase of pen-pressure sensor φ_{init} defines delay calibration phase in Fig. 13. During this phase, reference frequency of 500 kHz, TX_{ref} is applied to TX electrode, resonance in the ECR pen starts, and RDC is calibrated using the reference frequency at the same time. As long as the phase difference between the input TX_{ref} and TX_{refd} (delayed TX_{ref} through RDC) becomes zero, RDC has same propagation delay with the period of the reference frequency, 2 μs. The propagation delay of the CSIC is inversely proportional to its bias current I_b which is corrected by the calibration loop similar to a PLL. I_1 supplies the minimum operable current of the RDC. The calibration loop corrects I_{cal} so that the phase difference becomes zero. After the calibration (φ_{init}), V_{cal} is held at a loop compensation capacitor C_c and then pen-pressure sensor senses f_r of the ECR pen with the calibrated RDC in sensing phase of pen-pressure sensor. Since PFD and charge pump in the calibrator are not additionally required but shared with building blocks in pen-pressure sensor, it is much less complex than other schemes like digital calibrators.

D. TX Driver

Fig. 14 shows the TX driver with high voltage driving capability. To overcome weak electric coupling compared with magnetic coupling, TX driving voltage is increased up to 12 V. In order to drive TX electrodes with higher voltage than a conventional CMOS driver, high voltage rated output stage is

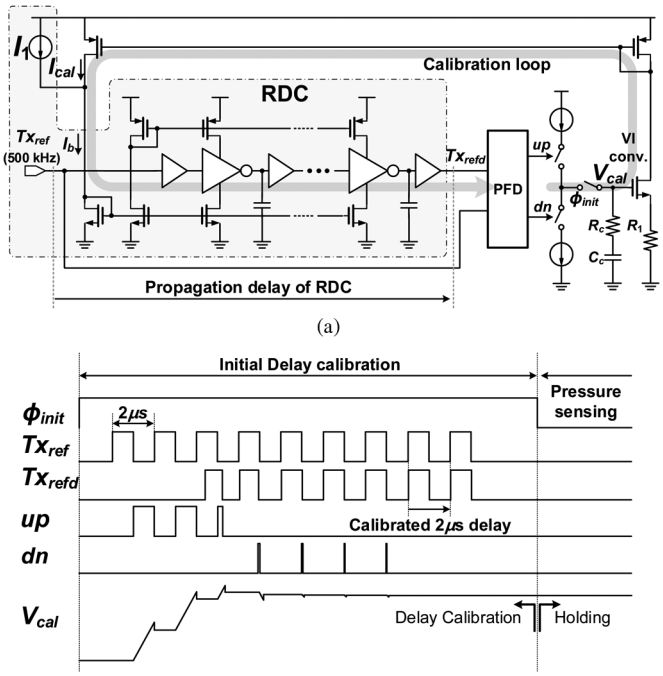

Fig. 13. (a) Proposed delay calibrator, and (b) its timing chart.

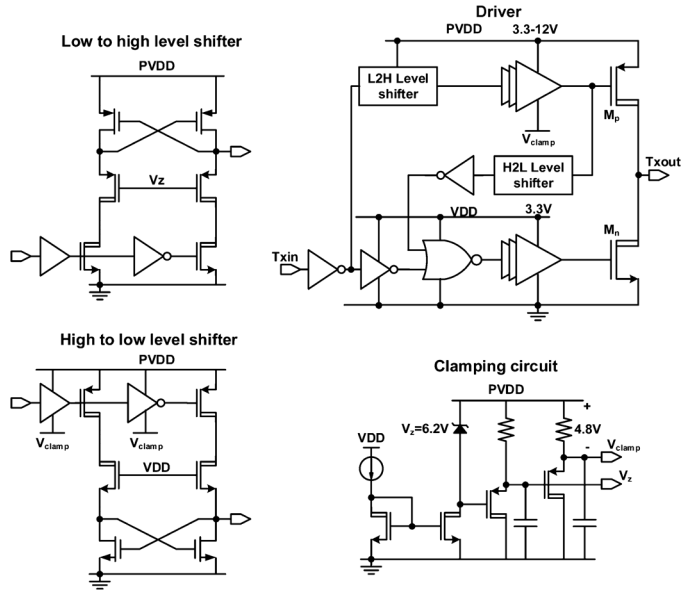

Fig. 14. Proposed TX driver.

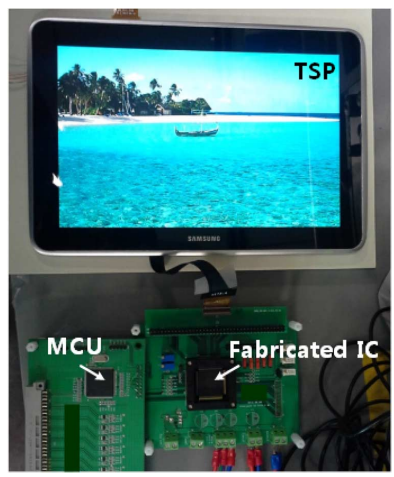

Fig. 15. Measurement setup for the experimental verification.

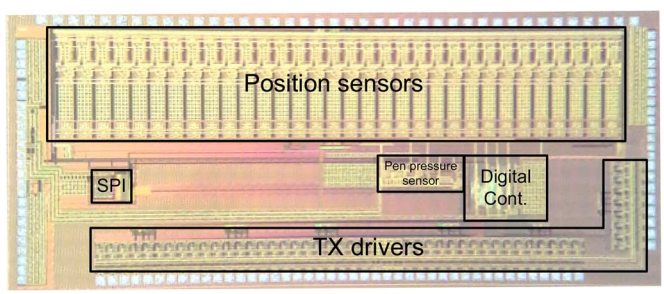

Fig. 16. Chip micrograph.

needed for the TX driver. Hence LDMOSes are used for output stage $(\mathrm{M_n}, \mathrm{M_p})$ of the driver. V_{ds} rating of LDMOS is quite high enough, but its V_{gs} rating is limited to 5 V for a reliable operation. Simple clamping circuit composed of source followers and Zener diode limits V_{gs} rating of LDMOS. To prevent shoot through current at the output stage, high to low (H2L) level shifter and NOR gate is inserted. In the turning-off process ($Txin$ goes low), $\mathrm{M_n}$ is turned on and $\mathrm{M_p}$ is turned off. $\mathrm{M_n}$ should be turned on after $\mathrm{M_p}$'s turning off to prevent shoot through. Since the propagation delay of a low to high (L2H) level shifter is always slower than propagation delay from $Txin$ to gate of $\mathrm{M_n}$, H2L level shifter and NOR gate is inserted to guarantee dead-time. If $\mathrm{M_p}$ is not turned off, NOR gate blocks $\mathrm{M_n}$'s turning on. In the turning-on process ($Txin$ goes high), $\mathrm{M_n}$ is turned off and $\mathrm{M_p}$ is turned on. Since the propagation delay of a low to high level shifter is always slower than propagation delay from $Txin$ to gate of $\mathrm{M_n}$, $\mathrm{M_p}$ is turned on later than $\mathrm{M_n}$'s turning off; shoot through is inherently eliminated.

V. Experimental Verifications

Measurement setup is shown in Fig. 15. 10.1″ commercial TSP is used. An MCU controls a fabricated IC, and calculates coordinates of touched object and applied pen-pressure on the ECR pen. The implemented IC is fabricated in 180 nm BCD process. A chip micrograph is shown in Fig. 16.

Waveforms of multi-TX driving patterns based on the modified $\boldsymbol{H}_8$, the output voltages of CDI of position sensor Vps for touched and untouched conditions with 6 mm φ metal pillar are shown in Fig. 17(a). Read-out touch image is shown in Fig. 17(b), and it shows touched positions where three types of metal pillars of 1 mm φ and 2 mm φ as a pen, and 6 mm φ as a finger are touched on TSP. The measured SNRs for 1 mm φ, and 6 mm φ metal pillars are 49 dB and 62 dB, respectively. Touch linearity measurement results are shown in Fig. 17(c) and (d). The diagonal is dawn on TSP and error between an actual drawn line and calculated coordinates is measured. The measured average linearity error is 0.0209 of TSP pattern pitch (4 mm). Waveforms of pen-pressure sensor are shown in Fig. 18(a), where the f_r of ECR pen is lower than

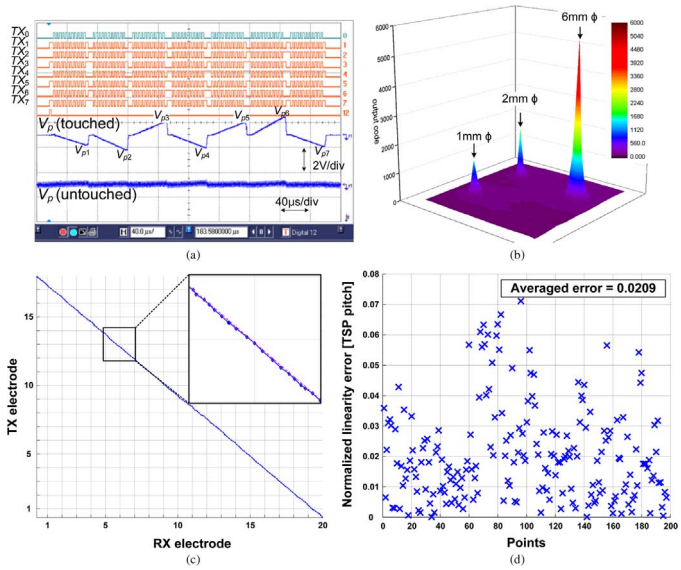

Fig. 17. Measurement results for position sensor. (a) Multi-TX pattern and V_p of CDI. (b) Constructed touch image. (c) Drawn straight line to evaluate touch linearity. (d) Normalized linearity error of (c).

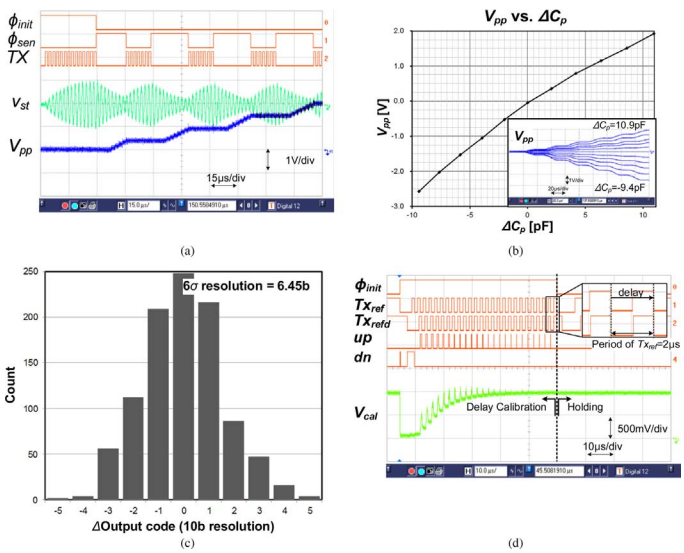

Fig. 18. Measurement results of pen pressure sensor. (a) Transient waveforms. (b) V_{pp} versus ΔC_p. (c) V_{pp} spread over 1000 samples, and (d) transient waveforms of the delay calibration.

the reference frequency of 500 kHz. The monotonicity of pen pressure corresponding voltage V_{pp} versus ΔC_p derived in (9) is verified by measurements as shown in Fig. 18(b). From this curve, the applied pen pressure on the ECR pen can be calculated. Measured V_{pp} spread on 1000 samples proves the pen-pressure sensing resolution of 6.45 bit on 6σ criteria as shown in Fig. 18(c). Waveforms for the delay calibration is shown in Fig. 18(d). The calibration voltage V_{cal} settles within φ_{init} And is held after the calibration.

VI. Conclusion

The performances of the proposed work and previous arts are summarized in Table I. By means of multi-TX scheme, the proposed touch system achieves quite high SNR even with 1 mm φ metal pillar to support the ECR pen and stable position sensing against external noise sources. The pen-pressure sensor senses variation of the pen-pressure-sensitive resonant capacitor in the ECR pen by sensing the resonant frequency f_r. The proposed capacitive touch system introduces a new and cost-effective pen-pressure sensitive passive pen solution using the ECR pen and pen-pressure sensor on a single capacitive TSP without additional sensing board.

TABLE I
Performance Summary

	ISSCC 2013 [6]	ISSCC 2013 [7]	ISSCC 2014 [8]	ISSCC 2014 [12]	This work
Process	350nm CMOS	180nm CMOS	350nm CMOS	180nm CMOS	180nm BCD
Pen pressure	N/A	N/A	N/A	N/A	**Support (6.5 bit)**
TSP Size	10.1"	-	4.5"	-	10.1"
TSP type	Mutual	Mutual	Mutual	Mutual	Mutual
# of channels	Tx : 27 Rx : 43	Tx : 30 Rx : 24	Tx:80 Rx:80	Tx : 24 Rx : 16	Tx : 48 Rx : 32
Scan rate	120 Hz	240 Hz	322Hz	160Hz	120 Hz
SNR	39dB (finger)	1mmϕ 35dB finger 55dB	1mmϕ 32dB finger 41dB	53 dB (finger)	1mmϕ 49dB 6mmϕ 62dB
Power	18.7mW	52.8mW	21.8mW	2.6mW	30mW
Chip area	10.4mm^2	14.9mm^2	6.25mm^2	0.46 mm^2 (Active)	14.7mm^2

References

[1] R. B. Mudit and V. B. Anand, "Comparative study of various touch-screen technologies," *Int. J. Comput. Appl.*, vol. 6, no. 8, pp. 12–18, Sep. 2010.

[2] G. Barret and R. Omote, "Projected-capacitive touch technology," *Information Display*, vol. 26, no. 3, pp. 16–21, Mar 2010.

[3] S. Ko, H. Shin, J. Lee, H. Jang, B.-C. So, I. Yun, and K. Lee, "Low noise capacitive sensor for multi-touch mobile handset's applications," in *IEEE A-SSCC*, Nov. 8–10, 2010, pp. 1–4.

[4] I.-S. Yang and O.-K. Kwon, "A touch controller using differential sensing method for on-cell capacitive touch screen panel systems," *IEEE Trans. Consumer Electronics*, vol. 57, no. 3, pp. 1027–1032, Aug. 2011.

[5] K.-D. Kim *et al.*, "A fully-differential capacitive touch controller with input common-mode feedback for symmetric display noise cancellation," in *IEEE SOVC*, June 10–13, 2014, pp. 1–2.

[6] J.-H. Yang *et al.*, "A highly noise-immune touch controller using filtered-delta-integration and a charge-interpolation technique for 10.1-inch capacitive touch-screen panels," in *ISSCC*, Feb. 2013, pp. 390–391.

[7] H. Shin, S. Ko, H. Jang, I. Yun, and K. Lee, "A 55 dB SNR with 240 Hz frame scan rate mutual capacitor 30 × 24 touch-screen panel read-out IC using code-division multiple sensing technique," in *ISSCC*, Feb. 2013, pp. 388–389.

[8] N. Miura *et al.*, "1 mm-pitch 80 × 80-channel 322 Hz-frame-rate touch sensor with two-step dual-mode capacitance scan," in *IEEE ISSCC*, Feb. 2014, pp. 216–217.

[9] Wacom, EMR Technology [Online]. Available: http://www.wacom-components.com/english/technology/emr.html

[10] Samsung, Galaxy note3+Gear [Online]. Available: http://www.samsung.com/global/microsite/galaxynote3-gear/

[11] N-trig, DuoSense Active Pen [Online]. Available: http://www.n-trig.com/Content.aspx?Page=DuoSense ActivePen

[12] H. Jang, H. Shin, S. Ko, I. Yun, and K. Lee, "2D coded-aperture-based ultra-compact capacitive touch-screen controller with 40 reconfigurable channels," in *IEEE ISSCC*, Feb. 2014, pp. 218–219.

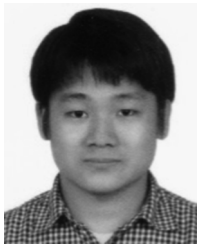

Changbyung Park received the B.S., M.S., and Ph.D. degrees in electrical engineering from the Korea Advanced Institute of Science and Technology (KAIST), Daejeon, Korea, in 2008, 2010, and 2015, respectively.

He is currently working in Digital Media and Communication R&D center, Samsung electronics, Suwon, Korea. He has worked on developing an LED driver IC and a column driver IC for LCD, and wireless power transfer system. His current research interests include wireless power transfer system and touch read-out circuit.

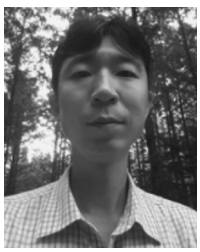

Sungsoo Park received the B.S. degree in electronics engineering from Seoul National University, Seoul, Korea, in 1990. He received the M.S. and Ph.D. degrees in electrical engineering from POSTECH, Pohang, Korea, in 1992 and 1996, respectively.

Since then, he has been with Samsung Electronics, Suwon, Korea. His main area of research interest is user interaction solutions.

Ki-Duk Kim (S'14) received the B.S. degree with highest honors from Korea Aerospace University, Seoul, Korea, in 2007, and the M.S. degree from Korea Advanced Institute of Science and Technology (KAIST), Daejeon, Korea, in 2009, both in electrical engineering. Since 2014, he has been working toward the Ph.D. degree in electrical engineering at KAIST, Daejeon, Korea.

From 2009 to 2014, he was with the Samsung Electronics, Yongin, Korea, and worked on circuit and system designs for display driver IC and touch controller IC. The ICs that were architected and designed by him won six ISSCC, VLSI and SID presentations from 2009 to 2014. He also won the Bronze Medal in the Human-Tech Paper Awards hosted by Samsung Electronics in 2010, and received the First Prize Award in the Samsung Semiconductor Technical Paper in 2010 and 2011 (twice), and the Distinguished Paper Award in SID, 2011. Now, his research interests are focused on 3D touch system for next generation smartphone, QUHD AMOLED display driver, and high efficiency buck-boost DC-DC converter for power management system, in the field of CMOS analog integrated circuit design.

Mr. Kim has authored and co-authored over 10 journal publications and conference presentations in the solid-state circuits and display area including ISSCC, VLSI, SID, ASSCC, IEEE JSSC. He holds more than 30 U.S., European, Japanese, Chinese, and Korea patens.

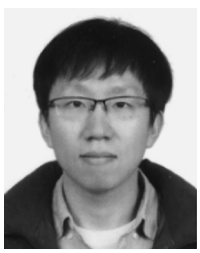

Sanghui Park (S'10) received the B.S. degree in electrical engineering from Korea University, Seoul, Korea, in 2010, and M.S. degree in electrical engineering from Korea Advanced Institute of Science and Technology (KAIST), Daejeon, Korea, in 2012. He is currently working toward the Ph.D. degree in electrical engineering at KAIST.

His research interests are in the field of analog integrated circuit design, including the design and modeling of touch screen readout circuits, switched capacitor circuits, power management IC and AMOLED display drivers.

Juwan Park received the M.S. degree in Interdisciplinary program for biomedical engineering from Seoul National University, Seoul, Korea, in 2006.

He joined Honeywell Analytics, Seoul, Korea, in 2006. Since 2012, he has been a Senior engineer in Digital Media & Communications R&D Center of Samsung Electronics, Suwon, Korea.

Byunghoon Kang received the Ph.D. degree in electrical engineering from the Pohang University of Science and Technology, Pohang, Korea, in 2013.

Since then, he has been with Samsung Electronics, Suwon, Korea, where he is currently the Senior Engineer of Digital Media & Communications R&D Center.

Yunhee Huh received the B.S. degree in electrical engineering from Sungkyunkwan University, Suwon, Korea, in 2013. She is currently working toward the Integrated Master and Ph.D. degree in electrical engineering at KAIST, Korea.

Her research interests are in the field of analog integrated circuit design, including the design and modeling of touch screen readout circuits, switched capacitor circuits, and power management IC.

Gyu-Hyeong Cho (S'76–M'80–SM'11) received the B.S. degree from Hanyang University, Korea, and the M.S. and Ph.D. degrees from the Korea Advanced Institute of Science and Technology (KAIST), Daejeon, Korea, in 1975, 1977, and 1981, respectively, all in electrical engineering.

During 1982–1983, he was with the Westinghouse R&D Center in Pittsburgh, PA, USA. In 1984, he joined the Department of Electrical Engineering at KAIST where he has been a full Professor since 1991. His early research was in the area of power electronics until the late 1990s and worked on soft switching converters and high power converters. Later, he shifted to analog integrated circuit design, and now he is interested in several areas including power management ICs, Class-D amplifiers, touch sensors and drivers for AMOLED and LCD flat panel displays, biosensors, and plasma power applications. He has authored one book on advanced electronic circuits and authored or coauthored over 200 technical papers and 80 patents.

Prof. Cho received the Outstanding Teaching Award from KAIST. He was a co-recipient of the Silkroad Award and guest editor at the ISSCC in 2007 and 2010, respectively. He also won Author-Recognition Award in 2013 as one of the top 16 contributors during last 60 years in ISSCC. He served as a member of the international technical program committees of ISSCC, and is now an associate editor of IEEE JOURNAL OF SOLID-STATE CIRCUITS.